Environmental Science Advances

ROYAL SOCIETY OF CHEMISTRY

PAPER

View Article Online
View Journal | View Issue

Cite this: *Environ. Sci.: Adv.*, 2026, **5**, 1328

Sustainable biomass-derived activated carbons from *Rosa brunonii* seeds for high-efficiency textile dye removal from water

Muhammad Bilal,*[a] Muhammad Idrees,[a] Javed Ali,[a] Amir Hossein Behroozi,[bf] Noushad Hussain,[a] Vahid Vatanpour[cde] and Tizazu H. Mekonnen *[f]

Sustainable activated carbons were produced from *Rosa brunonii* Lindl. seeds through physical activation (PAC) and chemical activation (CAC) routes and evaluated for the removal of representative textile dyes, Disperse Orange 1 (DO1) and Eriochrome Black T (EBT), from water. The activation process induced pronounced structural and chemical transformations, leading to porous carbon frameworks with enriched carbon content of approximately 93 wt% and excellent thermal stability. Adsorption experiments demonstrated that dye uptake is strongly influenced by initial dye concentration, solution pH, temperature, and adsorbent dosage, and particle size. The chemically activated carbon exhibited superior adsorption performance, particularly toward EBT, achieving a maximum capacity of 256.4 mg g^{-1}, whereas the PAC reached 192.3 mg g^{-1}. For DO1, adsorption capacities of 73.0 and 69.4 mg g^{-1} were obtained for PAC and CAC, respectively. Equilibrium adsorption behavior was best described by the Langmuir model, indicating predominantly monolayer adsorption, and the adsorption kinetics followed a pseudo-second-order model, suggesting strong dye–surface interactions. Adsorption was favoured at lower temperatures, consistent with an exothermic process. Solution pH had a pronounced effect on EBT adsorption, with maximum uptake under acidic conditions due to electrostatic attraction, whereas DO1 adsorption was largely pH independent. Overall, this study demonstrates the effective valorisation of agricultural waste into high-performance adsorbents and highlights *Rosa brunonii* seed-derived activated carbons as promising materials for sustainable textile wastewater remediation.

Received 24th December 2025
Accepted 9th March 2026

DOI: 10.1039/d5va00490j

rsc.li/esadvances

Environmental significance

This work presents a sustainable approach to textile wastewater treatment by converting discarded *Rosa brunonii* seeds into efficient activated carbons for dye removal. The biomass-derived adsorbents exhibit strong performance toward both disperse and anionic dyes, offering a low-cost and environmentally benign alternative to commercial activated carbons. By integrating agricultural waste valorization with water remediation, the study supports circular economy principles and addresses a critical challenge in sustainable pollution control.

1 Introduction

Industrialization has been a key driver of economic development, yet the rapid expansion of industrial activities has generated severe environmental challenges due to inadequate management of industrial wastes. Among these sectors, the textile industry is particularly problematic, as it is one of the most water-intensive manufacturing industries, especially during wet-processing operations such as dyeing and finishing. These processes typically consume 150–200 L of water per kilogram of textile produced[1] and generate large volumes of complex wastewater containing residual dyes, salts, auxiliary chemicals, and trace heavy metals.[2] Although more than 70 million tonnes of synthetic dyes are produced annually, incomplete fixation during textile processing results in the discharge of approximately 10–15% of dyes into effluents, corresponding to hundreds of thousands of tonnes released into aquatic environments each year.[3] Such dye-laden wastewaters are highly persistent and recalcitrant, imparting intense coloration even at low concentrations, reducing light penetration,

[a]*Department of Chemistry, Kohat University of Science and Technology, Kohat, 26000, KPK, Pakistan. E-mail: mbilal@kust.edu.pk*

[b]*Department of Chemical Engineering, Queen's University, Kingston, ON, K7L 3N6, Canada*

[c]*Department of Applied Chemistry, Faculty of Chemistry, Kharazmi University, 15719-14911, Tehran, Iran*

[d]*National Research Center on Membrane Technologies, Istanbul Technical University, Maslak, 34469, Istanbul, Türkiye*

[e]*Research Center for Environmental Chemistry and Green Development, Khazar University, Mahsati Str. 41, AZ-1096, Baku, Azerbaijan*

[f]*Department of Chemical Engineering, Institute of Polymer Research, University of Waterloo, Waterloo, ON N2L 3G1, Canada. E-mail: tmekonnen@uwaterloo.ca*

increasing chemical oxygen demand, and severely disrupting aquatic ecosystems.[4] Collectively, these impacts indicate the urgent need for advanced wastewater treatment strategies to mitigate the environmental consequences of dye-contaminated effluents.

Wastewater discharged from textile industries is typically characterized by intense coloration, elevated chemical and biological oxygen demand (COD and BOD), and an alkaline pH, reflecting its chemically complex nature. Such effluents often include a broad range of recalcitrant organic compounds, salts, and auxiliary chemicals utilized throughout dyeing and finishing processes, which further complicate treatment.[5] This complexity poses remarkable challenges for treatment, as conventional wastewater treatment plants often fail to completely remove synthetic dyes due to their high stability and resistance to biodegradation.[6] Textile dyes are broadly classified into reactive, disperse, direct, vat, sulfur, and acid dyes based on their solubility and application routes, with azo dyes accounting for nearly 70% of global dye production.[7] These dyes contain aromatic structures linked by azo (–N=N–) groups, which impart vivid and durable coloration but also confer pronounced environmental persistence.[8] Under anaerobic or reducing conditions, azo dyes may undergo reductive cleavage, which leads to the generation of aromatic amines that are often more toxic, mutagenic, and carcinogenic than the parent dye molecules.[9] Once discharged into aquatic environments, dyes can form light-blocking layers that inhibit photosynthesis, reduce dissolved oxygen levels, and disrupt aquatic food webs, ultimately leading to ecological degradation. Beyond their environmental impacts, dye contaminants compromise water aesthetics and quality, limit recreational and domestic use, and pose potential human health risks through bioaccumulation and trophic transfer.[10]

Among the numerous dyes released from textile effluents, Disperse Orange 1 (DO1) and Eriochrome Black T (EBT) are of environmental concern because of their widespread use and potential toxicity. DO1 is an azo-based disperse dye commonly applied in synthetic textile dyeing and has been reported as a sensitizing agent in humans, with evidence of cross-sensitization involving structurally related aromatic amines, such as 4-nitroaniline and *p*-aminodiphenylamine.[11] The persistence of DO1 in wastewater and its potential to generate hazardous transformation products further heighten concerns regarding its environmental release. EBT, an azo dye widely employed both as a metallochromic indicator in EDTA titrations[12] and as a textile colorant for fibers, such as wool, nylon, and silk,[13] poses notable health and environmental risks. Exposure to EBT-contaminated water has been associated with skin, ocular, respiratory, and gastrointestinal irritation, whereas prolonged contact may induce dermatitis and potential mutagenic effects.[14] Therefore, it is necessary to develop efficient and sustainable dye-removal strategies prior to wastewater discharge.

To mitigate the adverse impacts of such dyes, a variety of physical and chemical treatment methods have been investigated, including chemical precipitation, flocculation, oxidation, electrochemical processes, ion exchange, and adsorption.[15] Although these approaches can achieve partial or complete dye removal, many suffer from inherent limitations, such as high operational costs, incomplete mineralization, secondary sludge generation, and complex process requirements. Advanced oxidation processes, for instance, are effective in degrading dye molecules but often rely on high energy inputs and expensive reagents, restricting their large-scale implementation, particularly in resource-limited settings.[16] In contrast, adsorption has emerged as a highly attractive alternative due to its operational simplicity, cost-effectiveness, and environmental compatibility.[17,18] Importantly, adsorption enables efficient dye removal without producing substantial secondary waste, making it a promising and sustainable strategy for treating dye-contaminated textile effluents.[19]

Among available adsorbents, activated carbon remains the benchmark material for the removal of organic and inorganic contaminants from water and air owing to its high surface area, well-developed porous structure, and favorable surface chemistry.[20] However, the high production and regeneration costs associated with commercial activated carbon significantly limit its widespread application, particularly in large-scale wastewater treatment.[21] In response, growing attention has been directed toward the valorization of agricultural residues as low-cost precursors for activated carbon production.[22] Biomass-derived sources, such as fruit shells,[23] seeds,[24] husks,[25] offer renewable, economically viable alternatives while simultaneously addressing agricultural waste disposal challenges. This integrated approach aligns environmental remediation with resource sustainability, positioning biomass-based activated carbons as promising candidates for cost-effective treatment of dye-contaminated textile effluents. Despite extensive research on common agricultural wastes, several regionally abundant and lignocellulose-rich biomasses remain unexplored as potential precursors for activated carbon synthesis.

In this work, *Rosa brunonii* Lindl. seeds were investigated as a sustainable and underutilized biomass precursor for the preparation of physically and chemically activated carbons aimed at the removal of representative azo dyes, DO1 and EBT, from aqueous environments. *Rosa brunonii* is a widely distributed wild Rose, particularly abundant in mountainous and temperate regions, whose seeds are typically discarded as agricultural or forestry residue with no established value-added application. The seeds possess a high lignocellulosic and carbon content, low ash fraction, and dense organic structure, which are desirable characteristics for activated carbon production, yet their potential as an adsorbent precursor has not been previously reported. This study examines how different activation strategies influence the structural and surface properties of the resulting carbons and how these features govern their adsorption behavior. Batch adsorption experiments were used to evaluate the effects of solution pH, initial dye concentration, temperature, and adsorbent dosage, whereas kinetic and equilibrium modeling provided insight into the adsorption mechanisms. To the best of our knowledge, this work represents the first systematic investigation of activated carbons derived from *Rosa brunonii* seeds. By coupling biomass waste valorisation with dye remediation, this study

contributes to the development of sustainable and cost-effective materials for textile wastewater treatment.

2 Materials and methods

2.1 Materials

All chemicals and reagents used in this study were of analytical grade and were used as received without further purification. Disperse Orange 1 (DO1) and Eriochrome Black T (EBT) dyes were purchased from Sigma-Aldrich (Karachi, Pakistan). Orthophosphoric acid (H_3PO_4, ≥85%), sodium hydroxide (NaOH, ≥98%), hydrochloric acid (HCl, 37%), nitric acid (HNO_3, 65%), and sodium nitrate ($NaNO_3$, ≥99%) were also obtained from Sigma-Aldrich (Karachi, Pakistan). High-purity nitrogen gas was used to provide an inert atmosphere during carbonization. Distilled water was employed throughout all experiments.

2.2 Preparation of adsorbents

2.2.1 Pristine biomass. Seeds of *Rosa brunonii* Lindl. were collected from District Orakzai, Khyber Pakhtunkhwa, Pakistan, in October 2024. The collected seeds were thoroughly rinsed with distilled water to remove adhering dust and surface impurities and subsequently air-dried under sunlight for one week to eliminate residual moisture. The dried biomass was then ground into a fine powder using a mechanical grinder and further processed to obtain a uniform particle size prior to activation (Fig. 1).

2.2.2 Preparation of activated carbons. Physically activated carbon (PAC) was produced by carbonizing 5 g of the dried *Rosa brunonii* seed powder in ceramic crucibles at 600 °C for 2 h in a tubular furnace under a continuous nitrogen flow of 20 mL min^{-1} to maintain an inert atmosphere.[26] During physical activation, thermal treatment of the biomass induces dehydration, depolymerization, and progressive aromatization of the lignocellulosic constituents. The release of volatile species, including H_2O, CO, CO_2, and light hydrocarbons, generates voids within the carbon matrix, leading to the formation of initial micro- and mesoporous structures. Concurrently, condensation and rearrangement of carbon-rich fragments promote the development of disordered aromatic domains, resulting in a porous carbon framework with improved structural integrity and thermal stability.

For the preparation of chemically activated carbon (CAC), 5 g of the biomass was first impregnated with 50 mL of 0.1 mol per L H_3PO_4, corresponding to a biomass-to-acid impregnation ratio of 1 : 10 (w/v), defined here as the mass of dry biomass (g) to the volume of phosphoric acid solution (mL), and agitated at 250 rpm for 60 min. The impregnated biomass was then repeatedly washed with distilled water (typically 4–6 successive washing cycles) until a near-neutral pH (≈7) was attained, which was used as the stopping criterion for washing, followed by carbonization under the same conditions used for PAC synthesis.[27,28] Then, both PAC and CAC samples were sieved to obtain particle size fractions of 45–90 μm, 90–212 μm, and greater than 212 μm to unsure uniformity of the adsorbents for subsequent adsorption studies. The chemical activation with H_3PO_4 follows a more intricate mechanism dominated by acid-catalyzed dehydration, crosslinking modulation, and pore development. During the impregnation step, phosphoric acid penetrates the biomass matrix and interacts with hydroxyl groups present in cellulose, hemicellulose, and lignin, facilitating dehydration and cleavage of ether and ester linkages. These reactions inhibit tar formation during subsequent carbonization and promote the generation of thermally stable phosphate and polyphosphate intermediates. Upon heating, the phosphorus-containing species act as pore-directing agents, limiting structural shrinkage and fostering the formation of an

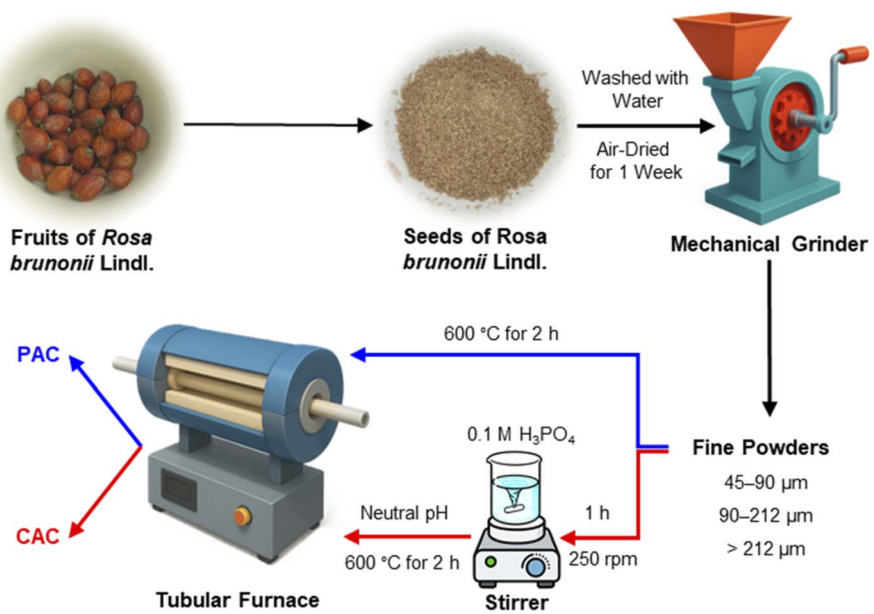

Fig. 1 Schematic preparation of PAC and CAC form seeds of *Rosa brunonii* Lindl.

interconnected porous network. The concurrent release of volatile byproducts, such as water vapor and low-molecular-weight oxygenated compounds, further contributes to pore expansion. Following carbonization, residual phosphorus species and soluble phosphate byproducts are removed during washing, leaving behind enlarged pores and surface oxygen functionalities that enhance the adsorption performance of the activated carbon.

2.3 Characterization of ACs

The raw biomass and the synthesized ACs were characterized using complementary analytical techniques. Surface functional groups were identified by Fourier transform infrared (FTIR) spectroscopy (Spectrum Two, PerkinElmer) over the range of 400–4000 cm^{-1}. Thermogravimetric analysis (TGA) was performed using a Diamond Series analyzer (PerkinElmer, USA) under a nitrogen atmosphere to evaluate thermal stability and carbonization behaviour, with the temperature ramped from 20 to 900 °C at a heating rate of 10 °C min^{-1}. Surface morphology and textural features were examined using scanning electron microscopy (SEM) (JSM-5910, JEOL, Japan) operated at an accelerating voltage of 10 kV and magnifications between 150× and 5000×. Elemental composition and surface elemental distribution were determined by energy-dispersive X-ray spectroscopy (EDX) using an INCA 200 system (Oxford Instruments, UK) coupled to the SEM. Crystallographic characteristics were analyzed using X-ray diffraction (XRD) (JDX-3532, JEOL, Japan) with Cu Kα radiation (λ = 1.5418 Å). UV-visible spectroscopy (Shimadzu UV-1800) was employed to quantify dye concentrations and evaluate adsorption performance, using a wavelength range of 190–800 nm and a slit width of 1.0 nm. Specific surface area measurements were performed using a NOVA 1200e gas sorption analyzer (Quantachrome Instruments, USA) based on nitrogen adsorption at 77 K, with BET analysis conducted over a relative pressure (P/P_0) range of 0.05–0.30.

The point of zero charge (pH_{PZC}) of the ACs was determined using the pH drift method. Briefly, 40 mL aliquots of 0.1 M $NaNO_3$ solution were adjusted to initial pH values between 2 and 12 using 0.1 M HNO_3 or 0.1 M NaOH. Activated carbon (0.1 g) was then added to each solution, and the suspensions were agitated at 250 rpm for 24 h. The final pH was recorded after equilibration, and the pH_{PZC} was identified as the pH at which the difference between initial and final pH (ΔpH) was zero, corresponding to a neutral surface charge.[29]

2.4 Adsorption experiments

The adsorption behaviour of Disperse Orange 1 (DO1) and Eriochrome Black T (EBT) on physically activated carbon (PAC) and chemically activated carbon (CAC) was systematically investigated through batch experiments by varying key operational parameters. The effects of initial dye concentration (5–1000 mg L^{-1}), solution pH (2–9, adjusted using 0.1 mol per L HCl and 0.1 mol per L NaOH), adsorbent dosage (0.1–0.5 g per 50 mL, corresponding to 2–10 g L^{-1}), contact time (up to 60 min), temperature (0–80 °C), and adsorbent particle size (90–212 μm) were evaluated. When one parameter was varied, all other parameters were maintained constant at pH 6.5–7.0, a contact time of 60 min (ensuring equilibrium), an adsorbent dosage of 0.1 g, an initial dye concentration of 50 mg L^{-1}, and a temperature of 25 °C. All experiments were conducted using 50 mL dye solutions under constant agitation (250 rpm), unless otherwise specified. Equilibrium adsorption data obtained at near-neutral pH (6.5–7.0) and 25 °C were analyzed using Langmuir and Freundlich isotherm models to elucidate adsorption behavior and surface characteristics of the adsorbents. Following the adsorption process, the solutions were filtered through Whatman No. 42 filter paper and residual dye concentrations were determined by UV-visible spectrophotometry following filtration. The performance of ACs was evaluated in terms of adsorption capacity (q_e, mg g^{-1}) measured by the following equation:[30]

$$q_e = \frac{(C_i - C_e)V}{m} \quad (1)$$

here, C_i and C_e (mg L^{-1}) represent the initial and equilibrium dye concentrations, V (L) is the aqueous solution volume, and m (g) is the adsorbent dosage. The characteristic absorption maxima of DO1 and EBT in UV-visible spectroscopy were located at 465 and 515 nm, respectively.

2.5 Kinetics and isotherm studies

Adsorption kinetics were evaluated using the pseudo-first order (PFO) and pseudo-second order (PSO) models to elucidate the rate-controlling mechanisms. The PFO model assumes that the adsorption rate is proportional to the number of unoccupied active sites and is described by the following equation:[31]

$$\log(q_e - q_t) = \log q_e - \frac{k_1}{2.303} t \quad (2)$$

where q_e and q_t (mg g^{-1}) represent the adsorption capacities at equilibrium and at time t, respectively, and k_1 (min^{-1}) is the PFO rate constant.

The PSO model, which presumes that adsorption follows a second-order mechanism with respect to the available sites, is expressed by the following equation:[31]

$$\frac{t}{q} = \frac{1}{k_2 q_e^2} + \frac{t}{q_e} \quad (3)$$

where k_2 (g mg^{-1} min^{-1}) denotes the PSO rate constant.

Equilibrium adsorption behavior was analyzed using the Langmuir and Freundlich isotherm models. The Langmuir model assumes monolayer adsorption on a homogeneous surface with finite identical sites and is given by the following equation:[31]

$$\frac{C_e}{q_e} = \frac{C_e}{q_m} + \frac{1}{K_L q_m} \quad (4)$$

where q_m (mg g^{-1}) is the maximum monolayer adsorption capacity and K_L (L mg^{-1}) is the Langmuir affinity constant.

The favorability of adsorption was further assessed using the dimensionless separation factor R_L, calculated according to the following equation:[31]

$$R_L = \frac{1}{1 + C_0 K_L} \quad (5)$$

where C_0 (mg L^{-1}) is the initial adsorbate concentration. The adsorption process is considered unfavorable when $R_L > 1$, linear when $R = 1$, favorable when $R_L < 1$.

The Langmuir constant K_L reflects the affinity between the adsorbate molecules and the adsorbent surface and is commonly associated with the adsorption energy. It is obtained from the slope and intercept of the linearized Langmuir plot and provides insight into the strength of adsorbate–adsorbent interactions.

The Freundlich model (eqn (6)) accounts for multilayer adsorption on energetically heterogeneous surfaces and is expressed as:

$$\log q_e = \log K_F + \frac{1}{n_F} \log C_e \quad (6)$$

where K_F and n_F are empirical constants related to adsorption capacity and intensity, respectively. Values of $0 < 1/n_F < 1$ indicate favorable adsorption.[31]

3 Results and discussion

3.1 Characterization of activated carbons

The surface morphology of the raw biomass and the derived activated carbons was investigated by SEM to assess the structural changes induced by carbonization and activation. As depicted in Fig. 2a, the untreated biomass exhibits a dense and relatively smooth surface with limited textural features, indicating the absence of a well-developed porous network prior to thermal treatment. After activation, substantial morphological transformations are observed. The PAC (Fig. 2b) shows a roughened surface with the formation of irregular cavities and fissures, which can be attributed to the thermal decomposition of lignocellulosic components and the release of volatile species during pyrolysis. In comparison, the CAC (Fig. 2c) prepared using H_3PO_4 displays a more pronounced and interconnected porous structure with widened pore openings and a sponge-like appearance, reflecting the role of acid in promoting dehydration, structural expansion, and pore development during carbonization. Overall, the enhanced surface accessibility and active site availability of PAC and CAC are favourable for adsorption applications in aqueous systems.

FTIR spectroscopy was employed to identify the surface functional groups present in the raw biomass and to assess the chemical transformations induced by carbonization and activation, as displayed in Fig. 3a. The spectrum of the raw biomass displays several characteristic bands associated with oxygenated and aliphatic functionalities. The broad band centered at approximately 3293 cm^{-1} corresponds to O–H stretching vibrations, indicating the presence of hydroxyl groups from alcohols, phenols, and adsorbed moisture.[32] The strong absorption at 2927 cm^{-1} is assigned to asymmetric C–H stretching of methylene groups, confirming the abundance of aliphatic hydrocarbons in the native biomass.[33] The band observed at 1731 cm^{-1} is attributed to C=O stretching vibrations of carbonyl groups, which may originate from aldehydes, ketones, or ester functionalities.[34] Additional bands at 1644 cm^{-1} and 1518 cm^{-1} are associated with C=C stretching of conjugated structures[35] and N–O stretching vibrations,[36] respectively, whereas the peak at 1456 cm^{-1} corresponds to C–H bending vibrations of methyl and methylene groups.[37] The bands at 1231 cm^{-1} and 1038 cm^{-1} are attributed to C–O stretching vibrations, consistent with the presence of ether, alcohol, and phenolic groups in the lignocellulosic framework.[38] Following carbonization, the FTIR spectra of PAC and CAC show a pronounced reduction in band intensity across the 3500 to 1600 cm^{-1} region, reflecting the extensive decomposition of hydroxyl, carbonyl, and aliphatic functional groups due to thermal treatment at 600 °C. The disappearance of the O–H

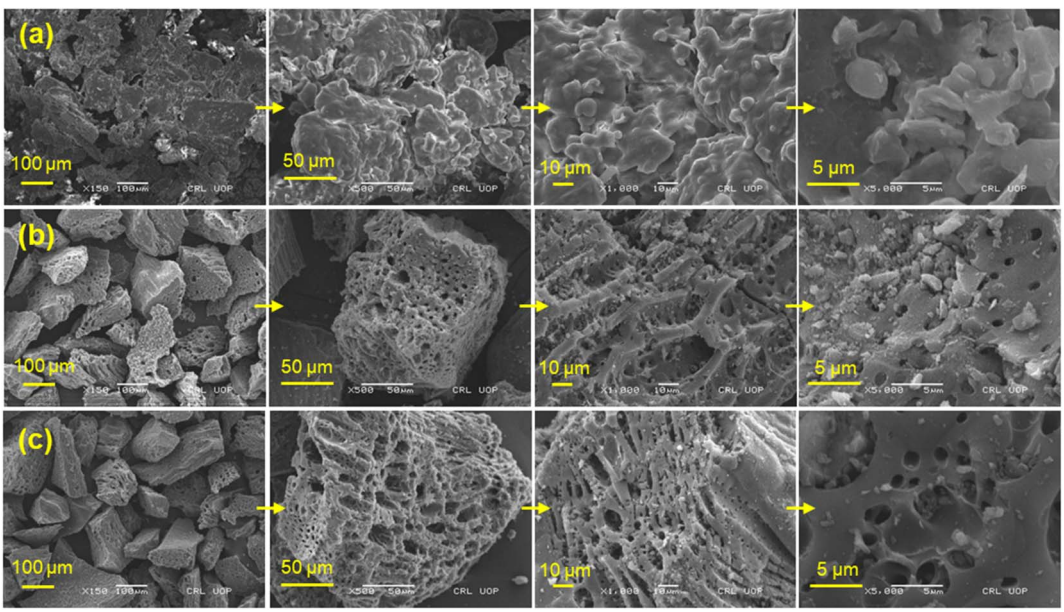

Fig. 2 SEM images of (a) raw biomass, (b) PAC, and (c) CAC samples.

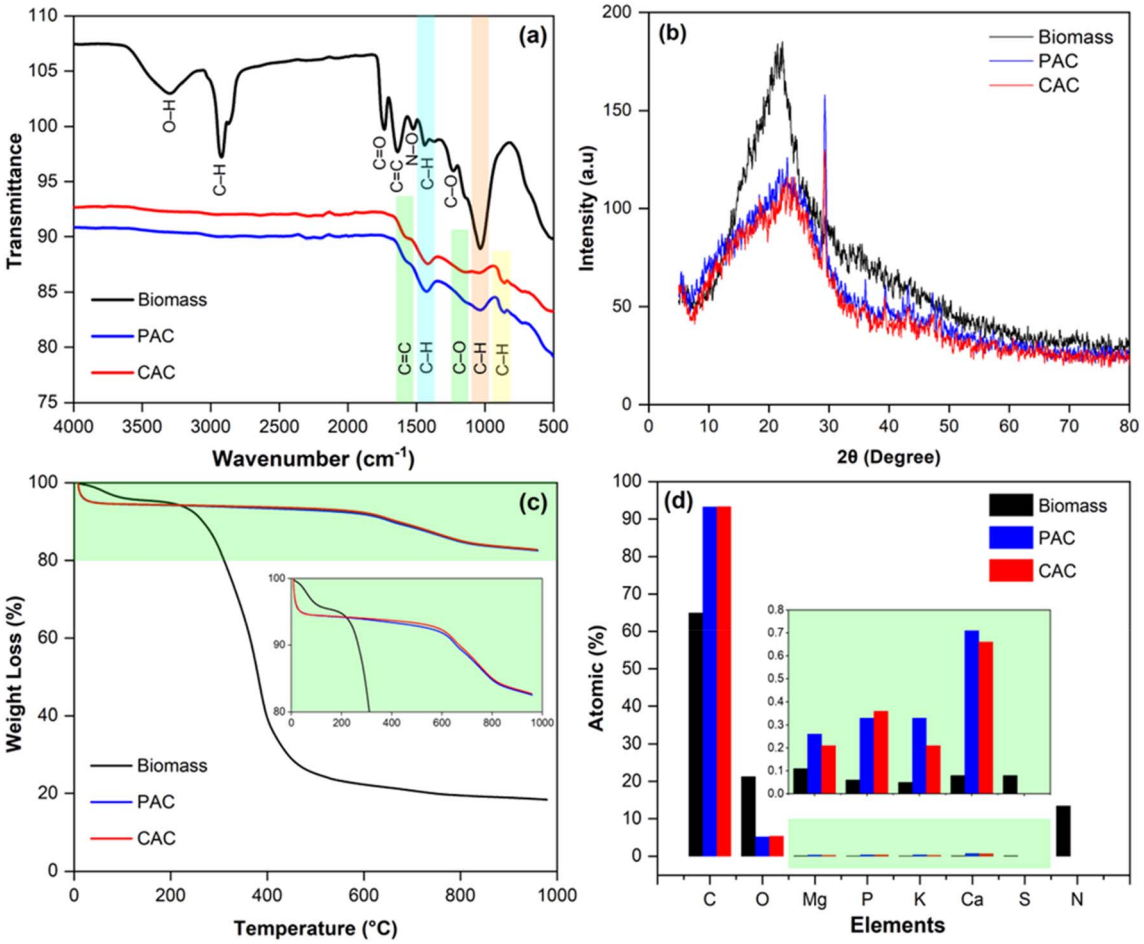

Fig. 3 Structural characterization of raw biomass, PAC, and CAC: (a) FTIR spectra, (b) XRD patterns, (c) TGA curves, and (d) elemental analysis based on EDX.

band and the strong attenuation of C–H stretching bands confirm effective devolatilization and aromatization of the carbon structure.[39] Both activated carbons exhibit weak bands near 1630 to 1520 cm^{-1}, which are attributed to C=C stretching within aromatic domains,[40] indicating the formation of a graphitized carbon framework. A small but distinct band observed around 1130 cm^{-1} in both PAC and CAC can be assigned to C–O stretching vibrations of phenolic or ether groups, while its slightly enhanced intensity in CAC likely reflects the contribution of phosphorus-containing oxygen functionalities formed during H_3PO_4 activation. Additionally, the weak band near 866 cm^{-1} corresponds to out-of-plane C–H bending vibrations of aromatic rings.[40] Overall, the substantial loss of oxygenated and aliphatic functionalities and the emergence of aromatic carbon structures confirm that carbonization and activation induced significant chemical bond cleavage and structural rearrangement, yielding activated carbons with chemically stable surfaces suitable for adsorption applications.

The XRD patterns of the activated carbons derived from *Rosa brunonii* Lindl. seeds are presented in Fig. 3b. Both PAC and CAC exhibit a broad diffraction feature centered near $2\theta \approx 21°$, which is characteristic of turbostratic or amorphous carbon with limited long-range crystalline order. The broadening and low intensity of this peak indicate a predominantly disordered carbon structure, whereas its slight shift toward higher angles suggests partial development of aromatic stacking during thermal treatment. Such structural evolution is commonly associated with progressive aromatization rather than true graphitization and is beneficial for creating a porous framework with abundant defect sites that enhance surface reactivity and adsorption performance.[41,42]

TGA was conducted to evaluate the thermal behavior of the raw biomass and to confirm the suitability of the selected carbonization temperature for producing stable activated carbons, as depicted in Fig. 3c. The activated carbon samples exhibit minimal mass loss, approximately 5%, below 100 °C, which is attributed to the removal of physically adsorbed moisture. Beyond this temperature, both PAC and CAC demonstrate excellent thermal stability, with only a gradual weight reduction observed up to 900 °C and a total mass loss of ~17%, indicating a highly carbonized and structurally reinforced framework. The high residual mass retained by PAC and CAC reflects their pre-carbonized nature and confirms that the selected carbonization temperature is sufficient to remove

volatile components while preserving a stable carbonaceous backbone. In contrast, raw biomass undergoes extensive thermal degradation, with an overall mass loss exceeding 80%. The initial weight reduction below 120 °C corresponds to moisture evaporation, followed by a major decomposition stage between 200 °C and 600 °C arising from the thermal breakdown of hemicellulose, cellulose, lignin, and other volatile organic constituents. At 600 °C, the biomass retained ~21 wt% of its initial mass under nitrogen, which is attributed to the formation of a carbonaceous char residue during inert pyrolysis. A final, slower degradation stage extending to 900 °C reflects the progressive decomposition of more thermally stable carbonaceous residues. The pronounced difference in thermal behavior between the raw precursor and the activated carbons confirms that carbonization and activation effectively transform the biomass into a thermally stable carbon material suitable for high-temperature and adsorption-based applications.[43,44]

The elemental composition of the materials was further examined by EDX analysis to confirm the formation and stability of the activated carbons, as shown in Fig. 3d. The EDX spectrum of the raw biomass indicates that it is primarily composed of carbon, oxygen, and nitrogen, with minor contributions from inorganic elements such as Mg, Al, K, and Ca, as well as trace amounts of P and S, which are commonly associated with naturally occurring mineral components. After carbonization and activation, a pronounced change in elemental composition is observed (Fig. 3d). The PAC and CAC consist predominantly of carbon and oxygen, with only trace levels of Mg, Al, Si, P, S, and Ca remaining, indicating effective removal of most noncarbonaceous constituents during thermal treatment. Quantitative analysis reveals a substantial increase in carbon content from 64.95% in the raw biomass to more than 93% in the ACs (both PAC and CAC), accompanied by a corresponding decrease in oxygen content from 21.27% to ~5%. Notably, nitrogen detected in the raw precursor is no longer observed after carbonization, reflecting the decomposition of nitrogen-containing organic moieties at elevated temperatures. These results confirm that pyrolysis at 600 °C promotes extensive devolatilization and aromatization, leading to the formation of a carbon-rich structure dominated by condensed aromatic domains. The high carbon content and reduced heteroatom concentration are expected to enhance structural stability and contribute to the favorable textural properties of the ACs.[45,46]

The BET surface area parameters of PAC and CAC (Table 1) were obtained from multi-point BET analysis (Fig. S1a, SI). CAC exhibits a higher monolayer adsorption capacity (W_m) and a correspondingly larger specific surface area (95.6 m^2 g^{-1}) compared with PAC (79.7 m^2 g^{-1}), indicating more effective pore development upon chemical activation. The BET constants for both materials (C_{BET} ≈ 3.9) are comparable, suggesting similar surface–adsorbate interaction energies for nitrogen adsorption at 77 K. The pore size distribution derived from nitrogen adsorption data is presented in Fig. S1b, indicating dominant pores at the micropore–mesopore boundary, with average pore radii of ~1.72 nm for PAC and ~1.89 nm for CAC and corresponding total pore volumes of 0.012 and 0.014 cm^3 g^{-1}, respectively. Overall, these results confirm that activation enhances the accessible surface area while preserving comparable adsorption energetics, which is consistent with the moderate surface heterogeneity expected for biomass-derived activated carbons.

Table 1 BET surface area parameters derived from linear BET analysis of PAC and CAC

Sample	W_m (g N_2 per g)	C_{BET}	S_{BET} (m^2 g^{-1})	V_p (cm^3 g^{-1})	r_p (nm)
PAC	0.0229	3.86	79.7	0.012	1.72
CAC	0.0275	3.94	95.6	0.014	1.89

The point of zero charge (pH_{PZC}) is a key interfacial parameter that describes the surface charge behaviour of an adsorbent and provides insight into its surface chemistry under varying pH conditions. It represents the pH at which the net surface charge of the material is zero and therefore governs electrostatic interactions between the adsorbent and charged species in solution. The pH_{PZC} values of the activated carbons were determined from the pH drift curves shown in Fig. 4. At very low pH values such as pH 2, the activated carbon surface becomes rapidly saturated with protons, limiting further proton uptake and resulting in a relatively small change in ΔpH. In contrast, at moderately acidic conditions around pH 4, surface functional groups are not fully protonated and actively participate in proton exchange, leading to a higher ΔpH. This behavior reflects the buffering capacity of oxygen-containing surface groups and their pK_a-dependent acid–base equilibria. The negative ΔpH minimum observed near pH 10 is attributed to the deprotonation of acidic surface groups, particularly phenolic and carboxylic functionalities, which release protons into the solution and lower the final pH. For both PAC and CAC, the intersection of the curves with the zero ΔpH line occurs at approximately pH 7.9, indicating identical pH_{PZC} values for the two materials. Although phosphoric acid activation is commonly associated with the introduction of acidic surface functionalities, extensive post-activation washing combined with subsequent thermal treatment can substantially diminish

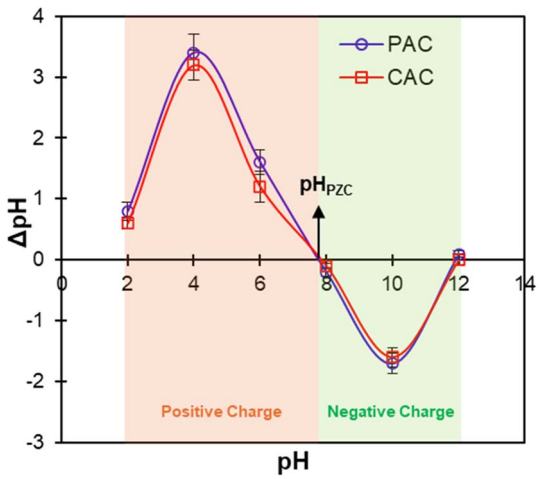

Fig. 4 Determination of pH_{PZC} of PAC and CAC adsorbents.

residual phosphate species on the carbon surface. As a result, the surface charge may shift toward near-neutral behavior, leading to pH_{PZC} values close to neutrality, as observed in the present study. This behavior is consistent with the findings of Rai *et al.*,[47] who reported a pH_{PZC} of 6.8 for mango kernel-derived activated carbon prepared using 40% H_3PO_4 after thorough washing to a neutral filtrate pH, demonstrating that near-neutral pH_{PZC} values are attainable for phosphoric-acid-activated biomass carbons following appropriate post-treatment. At solution pH values below 7.9, the surfaces of both activated carbons are predominantly positively charged, whereas at pH values above this value, the surface charge becomes increasingly negative. The near symmetry of the ΔpH extrema around the pH_{PZC} reflects the amphoteric nature of the activated carbon surface, with protonation dominating under acidic conditions and deprotonation prevailing in alkaline media.[48]

3.2 Effects of operating conditions on dye adsorption

The adsorption behaviour of the PAC and CAC activated carbons derived from *Rosa brunonii* Lindl. seeds were systematically investigated through a series of batch adsorption experiments. Key operational parameters, including initial dye concentration for isotherm analysis, contact time for kinetic evaluation, temperature, solution pH, adsorbent dosage, and particle size, were independently varied to assess their influence on adsorption performance and to elucidate the governing adsorption mechanisms.

3.2.1 Effect of temperature. To evaluate the effect of temperature on dye adsorption, batch experiments were conducted over a temperature range of 0 to 80 °C while keeping all other parameters constant. The range of temperatures examined in this study indicates both environmental and practical considerations. Lower temperatures are relevant to real-world wastewater treatment scenarios, such as cold-climate conditions or unheated storage tanks, where influent streams can approach near-freezing temperatures and adsorption performance under such conditions can influence design and operation.[49] Elevated temperatures, on the other hand, are pertinent to industrial effluents, particularly from textile, dyeing, and chemical processes, where effluent streams may be discharged at higher temperatures prior to cooling.[50] The results shown in Fig. 5a indicate that the adsorption capacities of both DO1 and EBT dyes on PAC and CAC decrease progressively with increasing temperature. At lower temperatures, particularly at 0 °C, the highest adsorption capacities were observed, ranging from approximately 22 to 45 mg g^{-1}. As the temperature increased, a continuous decline in dye uptake occurred, and at 80 °C the adsorption capacities decreased to about 4 to 8 mg g^{-1}. This temperature-dependent phenomenon suggests that the adsorption process is exothermic in nature, as elevated temperatures weaken the interactions between the dye molecules and the adsorbent surface, leading to reduced adsorption efficiency. Similar trends have been reported in previous studies on dye adsorption using activated carbon materials,[51] supporting the observed thermal behaviour of the present system.

3.2.2 Effect of pH. The effect of solution pH on the adsorption of DO1 and EBT onto PAC and CAC was investigated over a pH range of 2.0 to 9.0 under otherwise identical experimental conditions. As presented in Fig. 5b, the adsorption capacity of DO1 remained nearly constant across the studied pH range, indicating that pH has a negligible influence on its uptake. This trend can be attributed to the weak ionization of DO1 in aqueous media, which allows stable interactions with the adsorbent surface over a wide pH range. Similar pH-independent adsorption behaviour has been reported for structurally related disperse dyes, such as Disperse Orange 25, whose adsorption onto activated carbon was found to be largely unaffected by pH variations between 4 and 9, with optimal performance near neutral pH.[52] In contrast, the adsorption of EBT exhibited a strong dependence on solution pH. EBT contains sulfonate groups that remain negatively charged in aqueous solution,[53] classifying it as an anionic dye. At acidic pH values, both PAC and CAC surfaces are predominantly positively charged, as inferred from their pH_{PZC} value of 7.9, which promotes electrostatic attraction between the adsorbent and the anionic dye molecules.[54] As the solution pH increases, the density of positively charged surface sites decreases while negatively charged sites become more prevalent, leading to increasing electrostatic repulsion and a corresponding decline in adsorption capacity. Consequently, EBT adsorption decreases markedly as pH increases, dropping from approximately 45 mg g^{-1} at acidic pH to below 10 mg g^{-1} at pH values above 7. This trend is consistent with previous studies reporting maximum EBT adsorption under acidic conditions and diminished uptake in alkaline media.[55] The pronounced pH sensitivity of EBT adsorption confirms that electrostatic interactions play a dominant role in governing its adsorption behaviour, in agreement with the surface charge characteristics of the activated carbons determined from pH_{PZC} analysis.

3.2.3 Effect of adsorbent dosage. The influence of adsorbent dosage on the adsorption of DO1 and EBT dyes was evaluated by varying the amount of PAC and CAC from 0.1 to 0.5 g while keeping all other experimental parameters constant. The results (Fig. 5c) indicate that the adsorption capacity decreases with increasing adsorbent dosage for both dyes. This characteristic is commonly attributed to particle aggregation and overlap of adsorption sites at higher solid concentrations, which reduce the effective surface area available for adsorption and limit the accessibility of active sites. In addition, an increase in adsorbent dosage can lead to unsaturated adsorption sites due to a fixed amount of dye in solution, resulting in a lower uptake capacity per unit mass of adsorbent.[56] Similar trends have been reported for dye adsorption systems, where higher adsorbent loadings led to reduced adsorption capacity due to diffusion limitations and decreased utilization efficiency of the available adsorption sites.[57]

3.2.4 Effect of adsorbent size. Particle size is an important parameter influencing the adsorption performance and practical applicability of adsorbents. Although smaller particles generally offer higher surface area and shorter diffusion paths, they may cause pressure drop and clogging issues in fixed bed

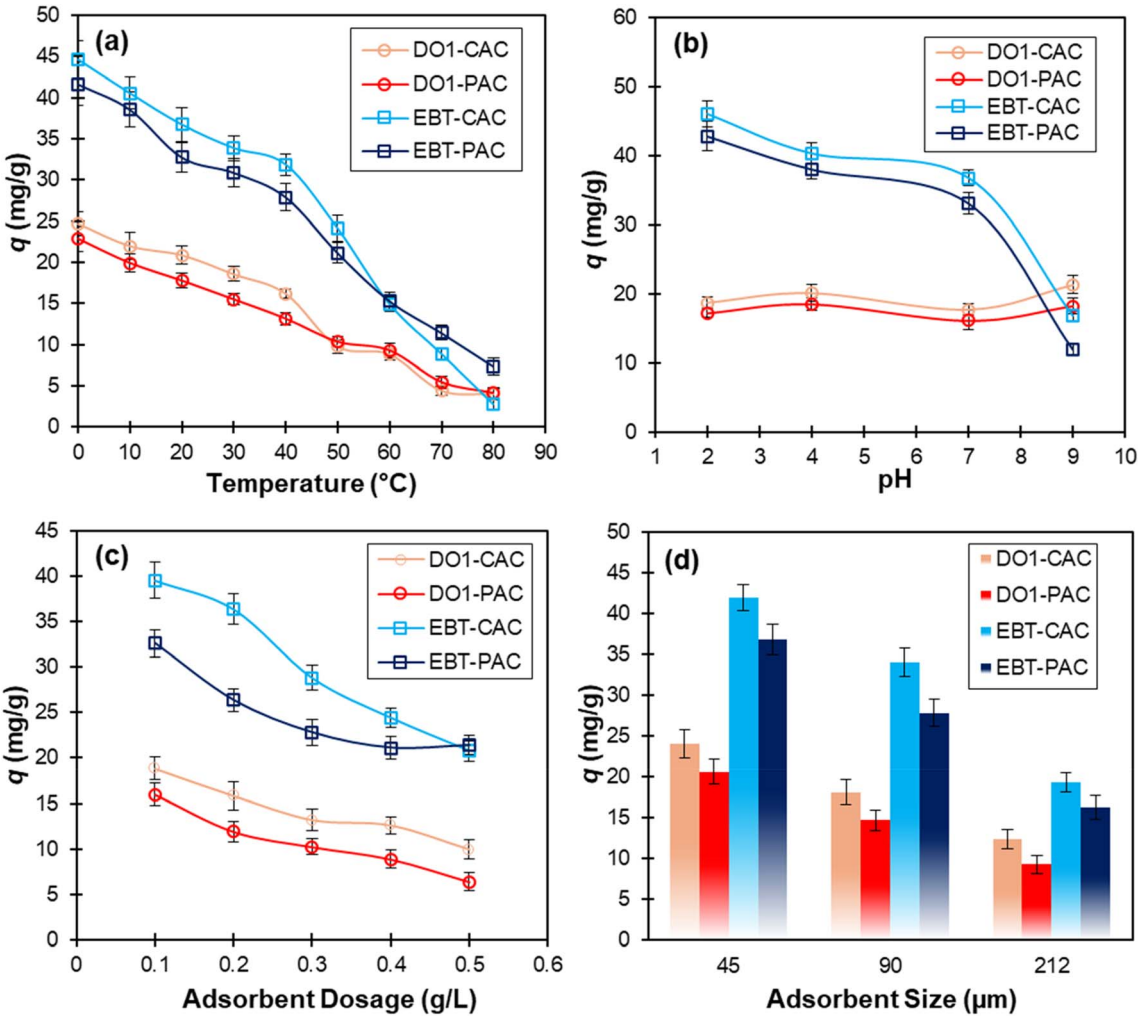

Fig. 5 Effects of operating conditions on the adsorption of DO1 and EBT onto PAC and CAC: (a) temperature (b) solution pH, (c) adsorbent dosage, and (d) adsorbent size.

systems, whereas larger particles often exhibit reduced adsorption efficiency due to limited surface accessibility. To determine an appropriate particle size for dye removal, adsorption experiments were conducted using three particle size fractions, namely 45 to 90 μm, 90 to 212 μm, and greater than 212 μm. As displayed in Fig. 5d, the adsorption capacity of both dyes decreases systematically with increasing particle size. The higher uptake observed for smaller particles can be ascribed to their larger external surface area and enhanced availability of active adsorption sites, which facilitate more effective dye diffusion and interaction with the adsorbent surface. In contrast, larger particles possess lower surface area to volume ratios and longer internal diffusion paths, which limit mass transfer and reduce overall adsorption efficiency.[58] These results highlight the importance of particle size optimization in achieving high adsorption performance while maintaining practical operability.

3.3 Kinetics and isotherm modelling

Adsorption kinetics and equilibrium behavior are key aspects for understanding the interaction between dye molecules and adsorbent surfaces, as well as for evaluating the efficiency and feasibility of adsorption processes. Kinetic studies provide insight into the rate of adsorption and the time required to reach equilibrium, which are critical parameters for process design and optimization. Isotherm analyses, on the other hand, describe how adsorbate molecules distribute between the solid and liquid phases at equilibrium and offer information on adsorption capacity, surface characteristics, and adsorption mechanisms.

The kinetic and isotherm data for the adsorption of DO1 and EBT onto PAC and CAC are presented in Fig. 6. The kinetic profiles in Fig. 6a show a rapid initial uptake of both dyes, followed by a gradual approach to equilibrium. For DO1, adsorption equilibrium was attained within approximately 30 min for both PAC and CAC, whereas EBT reached equilibrium much faster, within about 10 min, indicating a higher affinity of the activated carbon surfaces toward EBT molecules. Beyond these equilibrium times, further increases in contact duration resulted in negligible changes in adsorption capacity, and complete stabilization of the adsorption process was observed within ~60 min for all systems. Accordingly, a contact

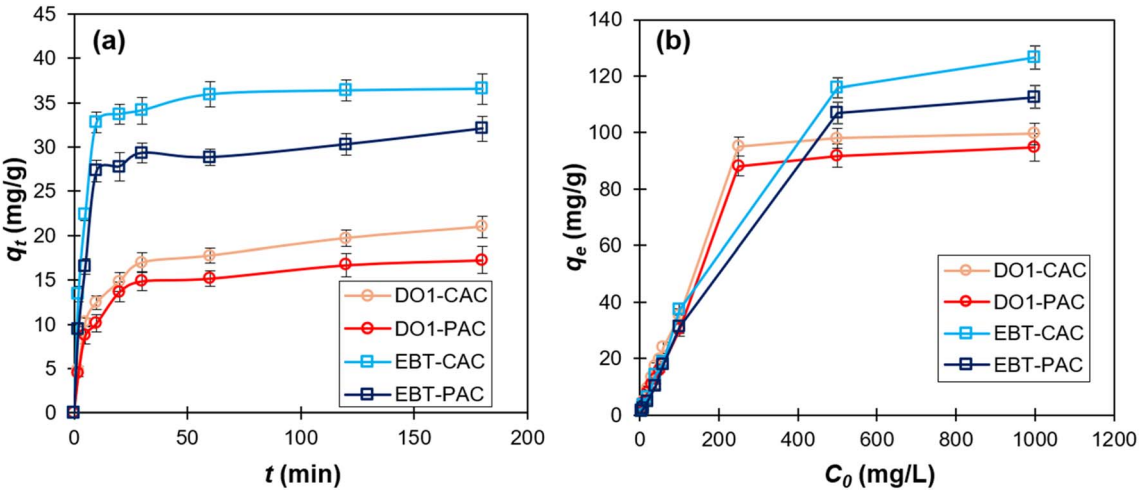

Fig. 6 Adsorption isotherm and kinetic data for DO1 and EBT on PAC and CAC: (a) kinetics; (b) isotherm.

time of 60 min was selected for all subsequent adsorption experiments to ensure that equilibrium was reached for every dye–adsorbent system and to allow meaningful and consistent comparison of adsorption performance across the different systems studied. The fast initial adsorption stage stems from the abundant availability of active surface sites on the activated carbons, which enables rapid interaction between dye molecules and adsorption sites. As adsorption proceeds, these sites become progressively occupied, leading to a reduced adsorption rate due to increased competition among dye molecules and diffusion limitations. This transition reflects a shift from surface-controlled adsorption at early stages to intraparticle and pore diffusion control at later stages, which is consistent with previously reported dye adsorption systems.[59] The equilibrium adsorption behavior is illustrated in Fig. 6b, where the adsorption capacity of both DO1 and EBT increases with increasing dye concentration for PAC and CAC. This trend is associated with the enhanced concentration gradient at higher initial dye concentrations, which provides a stronger driving force for mass transfer and promotes more efficient interaction between dye molecules and the adsorbent surface.[60]

The adsorption kinetics of DO1 and EBT on PAC and CAC were analyzed using the PFO and PSO kinetic models to elucidate the rate behavior and controlling mechanisms of the adsorption process. The linearized kinetic fittings are presented in Fig. 7, where Fig. 7a illustrates the PFO model and Fig. 7b shows the PSO model for both dyes on the two ACs. The corresponding kinetic parameters are summarized in Table 2. The PFO model provides a reasonable description of DO1 adsorption, with correlation coefficients (R^2) of 0.9186 for PAC and 0.9431 for CAC. However, the applicability of the PFO model to EBT adsorption is limited, particularly for EBT–PAC, where a markedly lower R^2 value of 0.7726 is obtained. In addition, the equilibrium adsorption capacities calculated from the PFO model differ substantially from the experimentally measured values, indicating that this model does not adequately represent the adsorption kinetics of EBT on the prepared activated carbons.

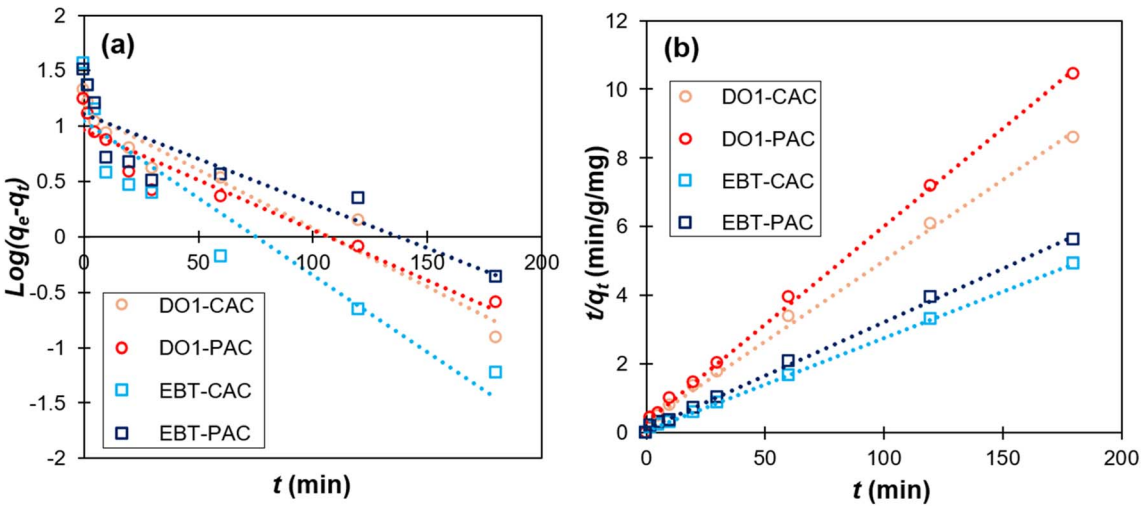

Fig. 7 Kinetic model fitting for DO1 and EBT adsorption on PAC and CAC: (a) PFO and (b) PSO models.

Table 2 Isotherm and kinetic parameters for the adsorption of DO1 and EBT on PAC and CAC

		DO1		EBT	
Model	Parameter	PAC	CAC	PAC	CAC
Langmuir	K_L (L mg^{-1})	0.021	0.114	0.003	0.004
	q_m (mg g^{-1})	72.99	69.44	192.31	256.41
	R_L	0.487	0.149	0.889	0.838
	R^2	0.9664	0.9928	0.9724	0.9952
Freundlich	n_F	1.604	1.926	1.186	1.363
	K_F	1.518	2.114	0.881	1.249
	R^2	0.9189	0.9122	0.9322	0.9326
PFO	k_1	0.021	0.024	0.018	0.032
	q_e	2.636	3.102	3.024	2.841
	R^2	0.9186	0.9431	0.7726	0.8740
PSO	k_2	0.011	0.007	0.009	0.013
	q_e	17.54	21.27	32.05	36.90
	R^2	0.9983	0.9967	0.9983	0.9997

In contrast, the PSO model exhibits excellent agreement with the experimental data for both dyes and both adsorbents, as shown in Fig. 7b. High correlation coefficients close to unity are obtained, with R^2 values of 0.9983 and 0.9967 for DO1 adsorption on PAC and CAC, respectively, and 0.9983 and 0.9997 for EBT adsorption on PAC and CAC. Moreover, the equilibrium adsorption capacities predicted by the PSO model closely match the experimental values, confirming the suitability of this model for describing the adsorption kinetics. The superior fitting of the PSO model suggests that the adsorption rate is governed by interactions between dye molecules and the available active sites on the activated carbon surfaces rather than by simple diffusion-controlled processes alone. Similar kinetic behavior has been widely reported for dye adsorption onto activated carbon materials,[61] where the PSO model consistently provides the best representation of experimental data.

The equilibrium adsorption behavior of DO1 and EBT on PAC and CAC was evaluated using the Langmuir and Freundlich isotherm models, with the corresponding linear fittings shown in Fig. 8 and the derived parameters summarized in Table 2. As illustrated in Fig. 8a, the Langmuir model provides an excellent fit to the experimental data for both dyes and both adsorbents, as evidenced by high correlation coefficients ranging from 0.9664 to 0.9952. The maximum monolayer adsorption capacities obtained from the Langmuir model demonstrate a markedly higher affinity of the activated carbons toward EBT compared to DO1, with q_m values of 192.31 and 256.41 mg g^{-1} for EBT on PAC and CAC, respectively, whereas DO1 exhibits lower capacities of 72.99 and 69.44 mg g^{-1}. The dimensionless separation factor RL values lie between 0 and 1 for all systems, confirming that adsorption is favorable over the studied concentration range.[62] The higher adsorption capacity observed for CAC, particularly toward EBT, arises from its more developed porous structure and greater availability of accessible adsorption sites.

The Freundlich isotherm model, which accounts for adsorption on heterogeneous surfaces with nonuniform site energies, was also applied to the equilibrium data, as illustrated in Fig. 8b. Although reasonable correlations were obtained, with R^2 values between 0.9122 and 0.9326, these values are consistently lower than those obtained from the Langmuir model, indicating a comparatively weaker description of the adsorption behaviour. The Freundlich constants n_F are greater than unity for all systems, indicating favourable adsorption, whereas the K_F values suggest enhanced adsorption affinity for CAC relative to PAC.[63] Overall, the isotherm analysis indicates that the equilibrium adsorption of both DO1 and EBT on the prepared ACs is best described by the Langmuir model, implying predominantly monolayer adsorption on relatively uniform surface sites under the investigated conditions.

3.4 Adsorption mechanisms

The plausible adsorption mechanisms governing the uptake of DO1 and EBT dyes onto PAC and CAC are schematically illustrated in Fig. 9 and arise from the synergistic contribution of multiple surface interactions. For DO1, adsorption is predominantly driven by hydrophobic interactions between the

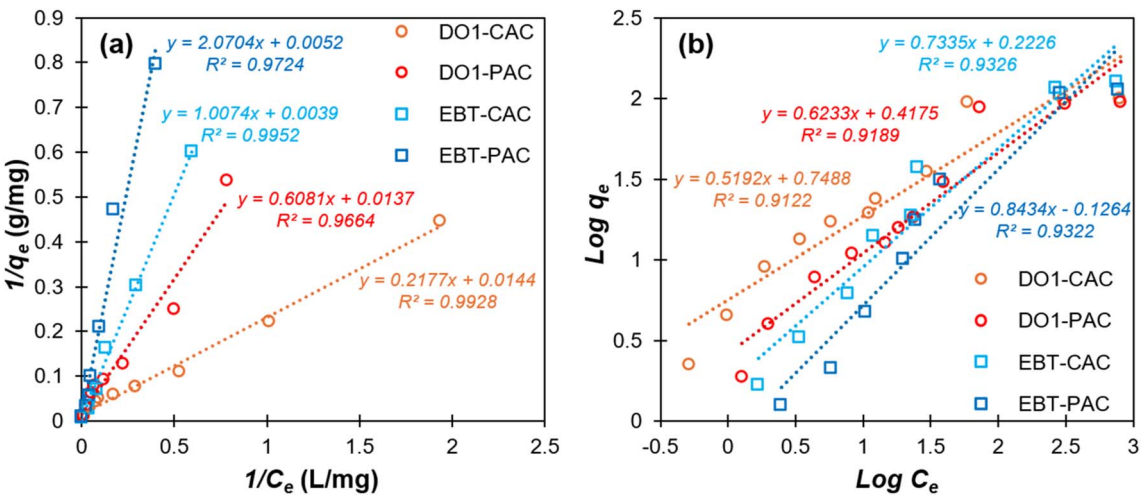

Fig. 8 Isotherm model fitting for DO1 and EBT adsorption on PAC and CAC: (a) Langmuir model; (b) Freundlich model.

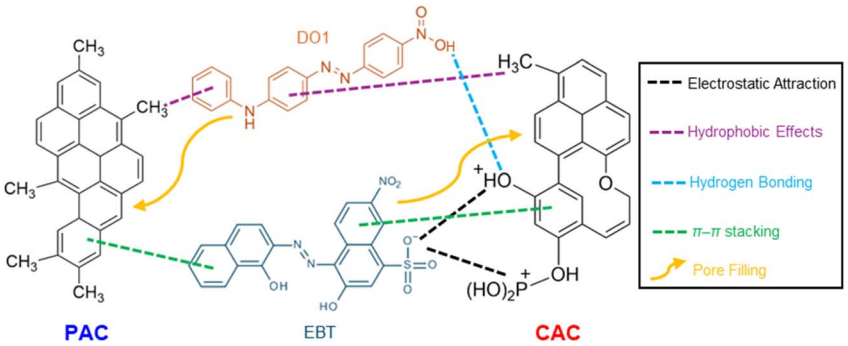

Fig. 9 Potential mechanisms of DO1 and EBT adsorption onto PAC and CAC adsorbents.

nonpolar aromatic backbone of the dye and the graphitized carbon domains of the activated carbons, which minimize interfacial free energy in aqueous media.[64] In parallel, strong π–π stacking interactions occur between the planar aromatic rings of DO1 and the conjugated sp^2-carbon structures present on PAC and CAC, facilitating favorable face-to-face alignment and stabilizing adsorption.[65,66] In addition, pore filling plays an important role in DO1 uptake, as the molecular dimensions of the dye enable its diffusion into the micro- and mesoporous network of the activated carbons, leading to physical confinement and enhanced retention within the pore structure.[19] Although the BET surface areas of PAC and CAC are moderate, the accessibility of the pore network allows effective utilization of the available internal surface, which supports efficient adsorption of aromatic molecules like DO1.[67] Notably, the higher adsorption capacity of DO1 on PAC compared with CAC can be attributed to the more graphitized and less functionalized surface of PAC formed during physical activation, which enhances hydrophobic interactions and π–π stacking with nonpolar aromatic dyes.

In contrast, the adsorption of EBT involves a more complex combination of electrostatic and noncovalent interactions due to its anionic and highly polar nature. The sulfonate groups of EBT impart a negative charge in aqueous solution, promoting electrostatic attraction with positively charged surface sites on PAC and CAC at solution pH values below the pH_{PZC}.[57] Hydrogen bonding interactions further contribute to EBT adsorption through interactions between oxygen-containing functional groups on the activated carbon surface and the hydroxyl and sulfonate moieties of the dye.[68] These surface functional groups, which are enriched during chemical activation, increase surface polarity and provide favorable interaction sites, thereby enhancing dye affinity.[69] Additionally, π–π stacking between the aromatic rings of EBT and the graphitic regions of the carbons enhances adsorption through noncovalent electronic interactions.[60] Pore filling also contributes to EBT uptake, particularly in CAC, where chemical activation generates a more developed pore network and higher accessibility of internal adsorption sites. Moreover, the accessibility of the pore network facilitates diffusion of the relatively bulky EBT molecules, allowing effective interaction with internal adsorption sites even in materials with moderate BET surface areas. As a result, CAC exhibits a higher adsorption capacity for EBT than PAC (Table 3), reflecting the dominant role of electrostatic attraction and hydrogen bonding associated with the higher surface functionality introduced by phosphoric acid activation. The combined contributions of electrostatic attraction, hydrogen bonding, π–π interactions, hydrophobic effects, and pore filling collectively account for the higher adsorption

Table 3 Comparative performance of different activated carbons for Disperse Orange and Eriochrome Black T dyes from water

Adsorbent	Dye	Optimal pH [pH_{PZC}]	Adsorbent dosage (g L^{-1})	Kinetics model	Isotherm model	q_{max} (mg g^{-1})	Ref.
AC from *Euphorbia rigida*	DO25	Independent [—]	1.2	PSO	Langmuir	118.9	52
Cenospheres/AC composite	DO25	6 [—]	0.3/0.1	PSO	Langmuir	90.9	70
AC from rattan sawdust	DO30	— [—]	0.3	—	Langmuir	133.3	71
AC from orange peel	DO7	2 [—]	0.75	PSO	Temkin	357.1	72
AC from *Rosa brunonii* Lindl. seeds	**DO1**	**Independent [7.9]**	**2**	**PSO**	**Langmuir**	**PAC: 73.0 CAC: 69.4**	**This work**
AC from waste hemp	EBT	3 [—]	0.4	PSO	Langmuir	14.0	73
AC from tea waste	EBT	2 [—]	11	PSO	Langmuir	151.3	55
AC from *Buxus wallichiana*	EBT	2 [5.9]	1	PSO	Freundlich	383.0	74
AC from *Spartium junceum*	EBT	— [7.2]	0.6	PSO	Langmuir	261.4	75
AC from *Datura metel* seeds	EBT	2 [—]	2	PSO	Langmuir	154.5	57
AC from *Rosa brunonii* Lindl. seeds	**EBT**	**6–7 [7.9]**	**2**	**PSO**	**Langmuir**	**PAC: 192.3 CAC: 256.4**	**This work**

capacity observed for EBT, especially on CAC, where surface functionality and porosity are more pronounced.

A comparative assessment of activated carbons reported in the literature for the adsorption of Disperse Orange and Eriochrome Black T dyes is summarized in Table 3. As shown, the activated carbons derived from *Rosa brunonii* Lindl. seeds in this work exhibit competitive and, in several cases, superior adsorption performance compared to previously reported biomass-based adsorbents. For DO dyes, the adsorption capacity achieved in this study is comparable to or higher than those reported for activated carbons prepared from rattan sawdust and cenosphere-based composites, while requiring a lower adsorbent dosage. More notably, for EBT adsorption, the prepared activated carbons demonstrate substantially higher maximum adsorption capacities, reaching 192.3 mg g^{-1} for PAC and 256.4 mg g^{-1} for CAC, outperforming many reported biomass-derived activated carbons under comparable or milder operating conditions. The superior performance of the present adsorbents can be attributed to their well-developed porous structure, high carbon content, and favorable surface chemistry, which collectively enhance dye–adsorbent interactions. These results highlight the effectiveness of *Rosa brunonii* Lindl. seed-derived activated carbons as promising and efficient materials for the removal of disperse and anionic dyes from aqueous systems.

4 Conclusions

This study demonstrates the successful valorization of *Rosa brunonii* Lindl. seeds into high-performance activated carbons prepared *via* physical and chemical activation routes and their effective application for the removal of hazardous dyes from aqueous media. Comprehensive structural and physicochemical characterization confirmed that thermal activation induces pronounced surface modification, pore development, and aromatization of the carbon framework. The prepared ACs reveal the formation of a predominantly amorphous to turbostratic carbon structure with high thermal stability up to 600 °C, accompanied by a substantial increase in carbon content to 93 at% and a marked reduction in oxygen content to about 5 at%. Chemical activation (CAC) produced a higher density of accessible surface functionalities, resulting in consistently enhanced adsorption performance relative to physically activated carbon (PAC), particularly for anionic dyes. Batch adsorption studies showed that dye uptake is governed by solution chemistry and material properties, including initial dye concentration, pH, and particle size. Equilibrium adsorption capacities reached 73.0 and 69.4 mg g^{-1} for DO1 on PAC and CAC, respectively, while significantly higher capacities were achieved for EBT, reaching 192.3 mg g^{-1} on PAC and 256.4 mg g^{-1} on CAC. The equilibrium data are best described by the Langmuir isotherm, indicating predominantly monolayer adsorption on relatively uniform surface sites, whereas the adsorption kinetics follow the pseudo-second-order model, reflecting strong dye–surface interactions. Adsorption was favoured at lower temperatures, consistent with an exothermic process. Solution pH played a critical role in EBT adsorption, with optimal uptake under acidic conditions due to electrostatic attraction, whereas DO1 adsorption remained largely pH independent owing to its weak ionization behavior. From a practical perspective, the use of an abundant, underutilized biomass precursor and straightforward activation procedures suggests favorable cost potential compared with conventional commercial activated carbons. Overall, the superior adsorption performance, favorable kinetics (reaching equilibrium during only 60 min), and low adsorbent dosage requirements position *Rosa brunonii* seed-derived activated carbons as sustainable, low-cost, and efficient materials for dye remediation.

Author contributions

Muhammad Bilal: conceptualization, methodology, investigation, formal analysis, project administration, supervision, writing – original draft, writing – review & editing. Muhammad Idrees: methodology, investigation, formal analysis, writing – review & editing. Javed Ali: methodology, investigation, formal analysis, writing – review & editing. Amir Hossein Behroozi: conceptualization, methodology, investigation, formal analysis, project administration, supervision, writing – original draft, writing – review & editing. Noushad Hussain: methodology, investigation, formal analysis, writing – review & editing. Vahid Vatanpour: methodology, investigation, formal analysis, writing – review & editing. Tizazu H. Mekonnen: conceptualization, project administration, supervision, writing – review & editing.

Conflicts of interest

There are no conflicts of interest to declare.

Data availability

The supporting data has been provided as part of the main manuscript and supplementary information (SI). Supplementary information: Fig. S1 is further experimental detail. See DOI: https://doi.org/10.1039/d5va00490j.

Acknowledgements

The authors acknowledge and appreciate for financial support of Kohat University of Science and Technology, Kohat, KPK, Pakistan under ORIC Research and Development Fund Program (KUST/ORIC/22/2370). The authors also acknowledge the financial support of Natural Science and Engineering Research Council of Canada (NSERC). This research was conducted in part thanks to funding from the Canada Research Chairs Program.

References

1 Y. Liu, J. Chen, D. Duan, Z. Zhang, C. Liu, W. Cai and Z. Zhao, Environmental Impacts and Biological Technologies Toward Sustainable Treatment of Textile Dyeing Wastewater: A Review, *Sustainability*, 2024, **16**, 10867.

2 A. Aghashiri, S. Hashemian and F. K. Fotooh, Adsorption of erochrom black T AzO dye by nanocomposite of activated carbon from sugar beet and LaFeO3, *Desalin. Water Treat.*, 2021, **212**, 173–184.
3 A. M. Jorge, K. Athira, M. B. Alves, R. L. Gardas and J. F. Pereira, Textile dyes effluents: A current scenario and the use of aqueous biphasic systems for the recovery of dyes, *J. Water Process Eng.*, 2023, **55**, 104125.
4 S. Khan, T. Noor, N. Iqbal and L. Yaqoob, Photocatalytic dye degradation from textile wastewater: a review, *ACS Omega*, 2024, **9**, 21751–21767.
5 S. I. Siddiqui, R. Ravi, G. Rathi, N. Tara, S. ul-Islam and S. A. Chaudhry, Decolorization of textile wastewater using composite materials, *Nanomaterials in the Wet Processing of Textiles*, 2018, pp. 187–218.
6 S. I. Siddiqui and S. A. Chaudhry, Nanohybrid composite Fe2O3-ZrO2/BC for inhibiting the growth of bacteria and adsorptive removal of arsenic and dyes from water, *J. Cleaner Prod.*, 2019, **223**, 849–868.
7 S. H. Hashemi and M. Kaykhaii, in *Emerging Freshwater Pollutants*, Elsevier, 2022, pp. 267–287, DOI: 10.1016/B978-0-12-822850-0.00013-2.
8 S. Benkhaya, S. M'rabet and A. El Harfi, Classifications, properties, recent synthesis and applications of azo dyes, *Heliyon*, 2020, **6**, e03271.
9 K.-T. Chung, Azo dyes and human health: A review, *J. Environ. Sci. Health, Part C*, 2016, **34**, 233–261.
10 R. A. E.-G. Mansour, M. G. Simeda and A. A. Zaatout, Removal of brilliant green dye from synthetic wastewater under batch mode using chemically activated date pit carbon, *RSC Adv.*, 2021, **11**, 7851–7861.
11 L. Malinauskiene, E. Zimerson, M. Bruze, K. Ryberg and M. Isaksson, Sensitizing capacity of D isperse O range 1 and its potential metabolites from azo reduction and their cross-reactivity pattern, *Contact Dermatitis*, 2013, **69**, 40–48.
12 B. Rietzler, A. P. Manian, D. Rhomberg, T. Bechtold and T. Pham, Investigation of the decomplexation of polyamide/CaCl2 complex toward a green, nondestructive recovery of polyamide from textile waste, *J. Appl. Polym. Sci.*, 2021, **138**, 51170.
13 J. K. Sahoo, R. K. Sukla, A. Pradhan, S. K. Sahoo and J. Rath, Removal of Eriochrome Black T dye using Plant Based Bio-Adsorbent: A Review, *Lett. Appl. NanoBioScience*, 2024, **13**, 73.
14 S. Ali, Q. M. Hassan, C. Emshary and H. Sultan, Characterizing optical and morphological properties of Eriochrome Black T doped polyvinyl alcohol film, *Phys. Scr.*, 2020, **95**, 095814.
15 G. Bal and A. Thakur, Distinct approaches of removal of dyes from wastewater: A review, *Mater. Today: Proc.*, 2022, **50**, 1575–1579.
16 M. Bilal, A. H. Behroozi, R. Jahan, J. Ali and V. Vatanpour, Sustainable TiO2/Diospyros texana seed-derived activated carbon composites for rapid photodegradation of oxytetracycline and amoxicillin under visible light, *J. Chem. Technol. Biotechnol.*, 2025, **100**, 2371–2382.
17 A. Pal, S. Das, S. R. Paul, A. Debnath, D. Datta, R. Bhoi and M. Yılmaz, Cost analysis and adsorption efficiency of chemically activated biochar from rubber wood sawdust for ciprofloxacin removal in environmental remediation, *Biomass Convers. Biorefin.*, 2026, **16**, 84.
18 K. Valizadeh, A. Bateni, N. Sojoodi, M. R. Ataabadi, A. H. Behroozi, A. Maleki and Z. You, Magnetized inulin by Fe3O4 as a bio-nano adsorbent for treating water contaminated with methyl orange and crystal violet dyes, *Sci. Rep.*, 2022, **12**, 22034.
19 F. M. Mohamed, M. R. El-Aassar, O. M. Ibrahim, A. Elsayed, M. F. Alrakshy, M. Abdel Rafea and K. A. Omran, Effective removal of carcinogenic azo dye from water using zea mays-derived mesoporous activated carbon, *ACS Omega*, 2024, **9**, 13086–13099.
20 A. Sharma, D. Mangla and S. A. Chaudhry, Recent advances in magnetic composites as adsorbents for wastewater remediation, *J. Environ. Manage.*, 2022, **306**, 114483.
21 D. H. da Silva Santos, Y. Xiao, N. Chaukura, J. M. Hill, R. Selvasembian, C. L. S. Zanta and L. Meili, Regeneration of dye-saturated activated carbon through advanced oxidative processes: A review, *Heliyon*, 2022, **8**, e10205.
22 J. Zhang, C. Duan, X. Huang, M. Meng, Y. Li, H. Huang, H. Wang, M. Yan and X. Tang, A review on research progress and prospects of agricultural waste-based activated carbon: preparation, application, and source of raw materials, *J. Mater. Sci.*, 2024, **59**, 5271–5292.
23 V. Mozhiarasi and T. S. Natarajan, Bael fruit shell–derived activated carbon adsorbent: effect of surface charge of activated carbon and type of pollutants for improved adsorption capacity, *Biomass Convers. Biorefin.*, 2024, **14**, 8761–8774.
24 N. Theamwong, W. Intarabumrung, S. Sangon, S. Aintharabunya, Y. Ngernyen, A. J. Hunt and N. Supanchaiyamat, Activated carbons from waste Cassia bakeriana seed pods as high-performance adsorbents for toxic anionic dye and ciprofloxacin antibiotic remediation, *Bioresour. Technol.*, 2021, **341**, 125832.
25 A. Kheddo, L. Rhyman, M. I. Elzagheid, P. Jeetah and P. Ramasami, Adsorption of synthetic dyed wastewater using activated carbon from rice husk, *SN Appl. Sci.*, 2020, **2**, 2170.
26 E. Altintig, B. Sarici, D. Bozdag, T. Over Ozcelik, M. Karakas and H. Altundag, Application of Optimization Response Surface for the Adsorption of Methylene Blue Dye onto Zinc-coated Activated Carbon, *Environ. Monit. Assess.*, 2024, **196**, 682.
27 A. Namane, A. Mekarzia, K. Benrachedi, N. Belhaneche-Bensemra and A. Hellal, Determination of the adsorption capacity of activated carbon made from coffee grounds by chemical activation with ZnCl2 and H3PO4, *J. Hazard. Mater.*, 2005, **119**, 189–194.
28 A. Lim, J. J. Chew, L. H. Ngu, S. Ismadji, D. S. Khaerudini and J. Sunarso, Synthesis, characterization, adsorption isotherm, and kinetic study of oil palm trunk-derived activated carbon for tannin removal from aqueous solution, *ACS Omega*, 2020, **5**, 28673–28683.
29 S. Neusatz Guilhen, T. Watanabe, T. Tieko Silva, S. Rovani, J. Takehiro Marumo, J. Alberto Soares Tenório, O. Mašek

and L. Goulart de Araujo, Role of point of zero charge in the adsorption of cationic textile dye on standard biochars from aqueous solutions: selection criteria and performance assessment, *Recent Prog. Mater*, 2022, **4**, 1–30.

30 L. R. Arenas, S. R. Gentile, S. Zimmermann and S. Stoll, Nanoplastics adsorption and removal efficiency by granular activated carbon used in drinking water treatment process, *Sci. Total Environ.*, 2021, **791**, 148175.

31 S. Azizian and S. Eris, in *Interface Science and Technology*, Elsevier, 2021, vol. 33, pp. 445–509.

32 A. Bateni, K. Valizadeh, Y. Salahshour, A. H. Behroozi and A. Maleki, Fabrication and characterization of pectin-graphene oxide-magnesium ferrite-zinc oxide nanocomposite for photocatalytic degradation of diclofenac in an aqueous solution under visible light irradiation, *J. Environ. Manage.*, 2022, **324**, 116358.

33 H. Wang, R. Xie, J. Zhang and J. Zhao, Preparation and characterization of distillers' grain based activated carbon as low cost methylene blue adsorbent: Mass transfer and equilibrium modeling, *Adv. Powder Technol.*, 2018, **29**, 27–35.

34 P. Kaur, S. Kalpana, S. Kumar, A. Kumar and A. Kumar, Effect of various sodium hydroxide treatment parameters on the adsorption efficiency of rice husk for removal of methylene blue from water, *Emergent Mater.*, 2023, **6**, 1809–1824.

35 M. Mierzwa-Hersztek, K. Gondek, A. Nawrocka, H. Pinkowska, T. Bajda, J. Stanek-Tarkowska and M. Szostek, FT-IR analysis and the content of phenolic compounds in exogenous organic matter produced from plant biomass, *J. Elementol.*, 2019, **24**, 879–896.

36 J. K. Kabeya, N. K. Ngombe, P. K. Mutwale, J. B. Safari, G. G. Matlou, R. W. M. Krause and C. I. Nkanga, Antimicrobial capping agents on silver nanoparticles made via green method using natural products from banana plant waste, *Artif. Cells Nanomed. Biotechnol.*, 2025, **53**, 29–42.

37 N. Tolosa, K. Mendoza, D. L. Dumayas and J. M. D. De Silva, Preparation and characterization of activated carbon derived from Antidesma bunius L. in methylene blue removal from wastewater, *J. Environ. Sci. Manage.*, 2020, 0119.

38 M. Tsarpali, J. N. Kuhn and G. P. Philippidis, Hydrothermal carbonization of residual algal biomass for production of hydrochar as a biobased metal adsorbent, *Sustainability*, 2022, **14**, 455.

39 J. Zhuang, M. Li, Y. Pu, A. J. Ragauskas and C. G. Yoo, Observation of potential contaminants in processed biomass using fourier transform infrared spectroscopy, *Appl. Sci.*, 2020, **10**, 4345.

40 P. Feng, J. Li, H. Wang and Z. Xu, Biomass-based activated carbon and activators: preparation of activated carbon from corncob by chemical activation with biomass pyrolysis liquids, *ACS Omega*, 2020, **5**, 24064–24072.

41 A. I. Bakti, P. L. Gareso and N. Rauf, Characterization of active carbon from coconut shell using X-ray diffraction (X-RD) and SEM-EDX techniques, *JPFA*, 2018, **8**, 115–122.

42 H. Khalil, M. Jawaid, P. Firoozian, U. Rashid, A. Islam and H. M. Akil, Activated carbon from various agricultural wastes by chemical activation with KOH: preparation and characterization, *J. Biobased Mater. Bioenergy*, 2013, **7**, 708–714.

43 C. Călin, E.-E. Sîrbu, M. Tănase, R. Győrgy, D. R. Popovici and I. Banu, A thermogravimetric analysis of biomass conversion to biochar: experimental and kinetic modeling, *Appl. Sci.*, 2024, **14**, 9856.

44 S. Szufa, M. Dzikuć, Ł. Adrian, P. Piersa, Z. Romanowska-Duda, W. Lewandowska, M. Marcza, A. Błaszczuk and A. Piwowar, Sustainable Drying and Torrefaction Processes of Miscanthus for Use as a Pelletized Solid Biofuel and Biocarbon-Carrier for Fertilizers, *Molecules*, 2020, **26**, 1014.

45 M. Amin, H. H. Shah, A. Iqbal, Z. U. R. Farooqi, M. Krawczuk and A. Zia, Conversion of waste biomass into activated carbon and evaluation of environmental consequences using life cycle assessment, *Appl. Sci.*, 2022, **12**, 5741.

46 T. S. Saleh, A. K. Badawi, R. S. Salama and M. M. M. Mostafa, Design and development of novel composites containing nickel ferrites supported on activated carbon derived from agricultural wastes and its application in water remediation, *Materials*, 2023, **16**, 2170.

47 M. K. Rai, G. Shahi, V. Meena, R. Meena, S. Chakraborty, R. S. Singh and B. N. Rai, Removal of hexavalent chromium Cr (VI) using activated carbon prepared from mango kernel activated with H3PO4, *Resour.-Effic. Technol.*, 2016, **2**, S63–S70.

48 M. Abdu, S. Babaee, A. Worku, T. A. Msagati and J. F. Nure, The development of Giant reed biochar for adsorption of Basic Blue 41 and Eriochrome Black T. azo dyes from wastewater, *Sci. Rep.*, 2024, **14**, 18320.

49 X. Zhang, Z. Wang, Y. Song, R. D. Tyagi and P. Drogui, in *Decentralized Sanitation and Water Treatment*, CRC Press, 2024, pp. 3–19.

50 D. Christian, A. Gaekwad, H. Dani, M. Shabiimam and A. Kandya, Recent techniques of textile industrial wastewater treatment: A review, *Mater. Today: Proc.*, 2023, **77**, 277–285.

51 M. H. Abdel-Aziz, E. Z. El-Ashtoukhy, M. Bassyouni, A. F. Al-Hossainy, E. M. Fawzy, S. M. Abdel-Hamid and M. S. Zoromba, DFT and experimental study on adsorption of dyes on activated carbon prepared from apple leaves, *Carbon Lett.*, 2021, **31**, 863–878.

52 Ö. Gerçel, H. F. Gerçel, A. S. Koparal and Ü. B. Öğütveren, Removal of disperse dye from aqueous solution by novel adsorbent prepared from biomass plant material, *J. Hazard. Mater.*, 2008, **160**, 668–674.

53 Y. S. Al-Degs, M. I. El-Barghouthi, A. H. El-Sheikh and G. M. Walker, Effect of solution pH, ionic strength, and temperature on adsorption behavior of reactive dyes on activated carbon, *Dyes Pigm.*, 2008, **77**, 16–23.

54 M. Alkhabbas, A. M. Al-Ma'abreh, G. Edris, T. Saleh and H. Alhmood, Adsorption of anionic and cationic dyes on activated carbon prepared from oak cupules: Kinetics and thermodynamics studies, *Int. J. Environ. Res. Public Health*, 2023, **20**, 3280.

55 M. Bansal, P. K. Patnala and T. Dugmore, Adsorption of Eriochrome Black-T (EBT) using tea waste as a low cost

adsorbent by batch studies: A green approach for dye effluent treatments, *Curr. Res. Green Sustainable Chem.*, 2020, **3**, 100036.

56 A. H. Behroozi, A. Mirahsani, P. Champagne and E. Koupaie, Protonated epichlorohydrin-crosslinked chitosan beads for ibuprofen removal from water: Insights into adsorption mechanisms, isotherms, kinetics, and reusability, *J. Contam. Hydrol.*, 2025, 104786.

57 J. Ali, E. M. Bakhsh, N. Hussain, M. Bilal, K. Akhtar, T. M. Fagieh, E. Y. Danish, A. M. Asiri, X. Su and S. B. Khan, A new biosource for synthesis of activated carbon and its potential use for removal of methylene blue and eriochrome black T from aqueous solutions, *Ind. Crops Prod.*, 2022, **179**, 114676.

58 A. M. Aljeboree, A. N. Alshirifi and A. F. Alkaim, Kinetics and equilibrium study for the adsorption of textile dyes on coconut shell activated carbon, *Arabian J. Chem.*, 2017, **10**, S3381–S3393.

59 M. Açıkyıldız, A. Gürses, K. Güneş and E. Şahin, Adsorption of textile dyes from aqueous solutions onto clay: Kinetic modelling and equilibrium isotherm analysis, *Front. Chem.*, 2023, **11**, 1156457.

60 B. M. Thamer, F. A. Al-Aizari and H. S. Abdo, Enhanced adsorption of textile dyes by a novel sulfonated activated carbon derived from pomegranate peel waste: isotherm, kinetic and thermodynamic study, *Molecules*, 2023, **28**, 7712.

61 C. H. Pimentel, M. S. Freire, D. Gómez-Díaz and J. González-Álvarez, Preparation of activated carbon from pine (Pinus radiata) sawdust by chemical activation with zinc chloride for wood dye adsorption, *Biomass Convers. Biorefin.*, 2023, **13**, 16537–16555.

62 Y. El Maguana, N. Elhadiri, M. Benchanaa and R. Chikri, Activated carbon for dyes removal: modeling and understanding the adsorption process, *J. Chem.*, 2020, **2020**, 2096834.

63 J. Fito, M. Abewaa, A. Mengistu, K. Angassa, A. D. Ambaye, W. Moyo and T. Nkambule, Adsorption of methylene blue from textile industrial wastewater using activated carbon developed from Rumex abyssinicus plant, *Sci. Rep.*, 2023, **13**, 5427.

64 N. Mittal, M. Kaur and V. Singh, Adsorption studies on hydrophobic disperse dye using cellulose derived mesoporous activated carbon, *Mater. Today: Proc.*, 2022, **62**, 7595–7599.

65 M. Kamau, S. Al-Najm and M. Nandeshwar, Recent advances in carbon-based nanocomposites for environmental remediation of industrial dyes, *Compos. Interfaces*, 2025, 1–34.

66 B. M. Choudhuri, K. Ramesh, A. Debnath and P. V. Chellam, Adsorptive removal of fluoroquinolones using bamboo culm biochar in a single and multi-component system, *Biomass Convers. Biorefin.*, 2025, 1–12.

67 S. Rudra Paul, S. Das, A. Debnath and T. Kumar Misra, Boosted adsorptive removal of eosin yellow dye from aqueous solution with C–ZnO nanoparticles: optimization of process parameters, *J. Dispersion Sci. Technol.*, 2026, **47**, 128–144.

68 J. Rath, J. K. Sahoo, R. K. Sukla, A. Pradhan, S. K. Biswal, P. Dwivedy and S. K. Sahoo, Eriochrome Black T dye removal from an aqueous solution using graphene oxide-modified activated carbon materials, *Indian Chem. Eng.*, 2024, **66**, 573–592.

69 A. H. Behroozi, P. Champagne, T. H. Mekonnen and E. Koupaie, Selective removal of anionic contaminants via porous polyethylene glycol-templated chitosan aerogel beads, *Sep. Purif. Technol.*, 2025, 136657.

70 M. Tiwari, S. Shukla and N. Dhiman, Characterization and adsorption of disperse dyes from wastewater onto cenospheres activated carbon composites, *Environ. Earth Sci.*, 2017, **76**, 702.

71 A. Ahmad, B. Hameed and A. Ahmad, Removal of disperse dye from aqueous solution using waste-derived activated carbon: Optimization study, *J. Hazard. Mater.*, 2009, **170**, 612–619.

72 A. Khalil, C. Mangwandi, M. A. Salem, S. Ragab and A. El Nemr, Orange peel magnetic activated carbon for removal of acid orange 7 dye from water, *Sci. Rep.*, 2024, **14**, 119.

73 F. El Mansouri, G. Pelaz, A. Morán, J. C. E. Da Silva, F. Cacciola, H. El Farissi, H. Tayeq, M. H. Zerrouk and J. Brigui, Efficient removal of eriochrome black T dye using activated carbon of waste hemp (Cannabis sativa L.) grown in northern Morocco enhanced by new mathematical models, *Separations*, 2022, **9**, 283.

74 M. Bilal, J. Ali, K. Bibi, S. B. Khan, M. Saqib, R. Saeed, R. Javeria, H. Khan, K. Akhtar and E. M. Bakhsh, Remediation of different dyes from textile effluent using activated carbon synthesized from Buxus Wallichiana, *Ind. Crops Prod.*, 2022, **187**, 115267.

75 A. Abiza, A. Reffas, H. Boubaker, R. Ben Arfi, D. Ghorbel, M. Rafique, G. L. Bachirou and A. Ghorbal, Comparative analysis of EBT dye removal using Spartium junceum and derived activated carbon: experimental and DFT insights, *Int. J. Environ. Anal. Chem.*, 2024, 1–27.